Predicting gait adaptations due to ankle plantarflexor muscle weakness and contracture using physics-based musculoskeletal simulations

Carmichael F. Ong[1], Thomas Geijtenbeek[2], Jennifer L. Hicks[1], Scott L. Delp[1,3,4*]

[1] Department of Bioengineering, Stanford University, Stanford, California, United States of America

[2] Department of Biomechatronics & Human-Machine Control, Delft University of Technology, Delft, The Netherlands

[3] Department of Mechanical Engineering, Stanford University, Stanford, California, United States of America

[4] Department of Orthopaedic Surgery, Stanford University, Stanford, California, United States of America

* Corresponding author

Email: delp@stanford.edu (SLD)

Abstract

Deficits in the ankle plantarflexor muscles, such as weakness and contracture, occur commonly in conditions such as cerebral palsy, stroke, muscular dystrophy, and Charcot-Marie-Tooth disease. While these deficits likely contribute to observed gait pathologies, elucidating cause-effect relationships is difficult due to the often co-occurring biomechanical and neural deficits. To elucidate the effects of weakness and contracture, we systematically introduced isolated deficits into a musculoskeletal model and generated simulations of walking to predict gait adaptations due to these deficits. We developed a planar model containing 9 degrees of freedom and 18 musculotendon actuators, and an optimization framework through which we imposed simple objectives, such as minimizing cost of transport while avoiding falling and injury, and maintaining head stability. We first validated that our model could generate gaits that reproduced experimentally observed kinematic, kinetic, and metabolic trends for two cases: 1) walking at prescribed speeds between 0.50 m/s and 2.00 m/s and 2) walking at self-selected speed. We then applied mild, moderate, and severe levels of muscle weakness or contracture to either the soleus (SOL) or gastrocnemius (GAS) or both of these major plantarflexors (PF) and retrained the model to walk at a self-selected speed. The model was robust to all deficits, finding a stable gait in all cases. Severe PF weakness caused the model to adopt a slower, "heel-walking" gait. Severe contracture of only SOL or both PF yielded similar results: the model adopted a "toe-walking" gait with excessive hip and knee flexion during stance. These results highlight how plantarflexor weakness and contracture may contribute to observed gait patterns. Our model, simulation and optimization framework, and results are freely shared so that others can reproduce and build upon our work.

Author summary

Deficits in the muscles that extend the ankle are thought to contribute to abnormal walking patterns in conditions such as cerebral palsy, stroke, muscular dystrophy, and Charcot-Marie-Tooth disease. To study how deficits in these muscles contribute to abnormal walking patterns, we used computer simulations to systematically introduce muscle deficits into a biomechanically accurate model. We first showed that our model could discover realistic walking patterns over a wide range of speeds when we posed a simple objective: walking while consuming a minimum amount of energy per distance, maintaining head stability, and avoiding injury. We then used the model to study the effect of two commonly observed problems: muscle weakness and muscle tightness. We found that severe weakness of the ankle extensors caused the model to adopt a slower, "heel-walking" gait, and severe tightness caused the model to adopt a crouched, "toe-walking" gait. These results highlight how deficits in the ankle extensor muscles may contribute to abnormal walking patterns commonly seen in pathological populations.

Introduction

The ankle plantarflexor muscles play an important role in human walking, and deficits in these muscles are thought to contribute to gait pathologies. Previous work has shown that the plantarflexor muscles are important for generating forward acceleration during the push-off phase of walking [1,2]. Individuals with cerebral palsy, stroke, muscular dystrophy, or Charcot-Marie-Tooth (CMT) disease often exhibit plantarflexor muscle weakness [3–9] and contracture [3,9–15]. However, these muscular deficits often co-occur with other abnormalities, such as skeletal deformities and neural deficits, making it difficult to assess the independent contributions of these muscular deficits to gait abnormalities.

Previous experimental work has sought to better understand the cause-effect relationship between plantarflexor weakness and gait pathologies by performing a tibial-nerve block in one leg in healthy subjects [16]. Adaptations on the affected side included a reduced ability to transfer weight to the contralateral leading limb during terminal stance and a shortened single-limb stance duration. Although this experiment helps to establish a cause-effect relationship, nerve blocks are invasive and thus difficult to repeat for many muscles. Further, these experiments cannot reveal the effects of contracture, which produces abnormally high passive stiffness of muscles.

Musculoskeletal simulations built from experimental gait data have been used to study gait pathologies. For example, simulations of individuals with cerebral palsy have quantified individual muscle contributions to body weight support and forward propulsion [17], the minimum muscle strength required to walk in a crouch gait [18], and the contributions of contracture and spasticity to increased hamstring resistance [19]. These studies suggest strong links between muscle deficits and the observed gait adaptations; however, since these studies tracked experimental data from patients with a combination of muscular, skeletal, and neural deficits, the independent effects of muscular weakness and contracture on the observed gait adaptations cannot be assessed.

Simulations in which kinematics are generated *de novo* (i.e., without tracking experimental data) can help reveal cause-effect relationships between muscular deficits and gait abnormalities. Researchers have created controllers that could generate various gait patterns, including level walking [20–23] and running [21,23], inclined walking [22,23], loaded walking [22], stair ascent, and turning [23]. More recently, Song and colleagues sought to understand which factors contributed to decreased walking performance in the elderly population [24]. By systematically introducing the neural, muscular, or skeletal deficits seen in this population and training each model to walk, they determined that decreased muscle strength and mass of all muscles contributed

most to typically observed gait adaptations. Although simulations of this type are valuable, they are not yet broadly used because it is challenging to generate simulations *de novo* and to reproduce previous work. Overcoming these challenges has been difficult because of the sensitivity of forward simulations to a software environment and limited sharing of software and models. More work is also needed to validate that simulations of this type capture the adaptations observed in experiments (e.g., due to varying walking speeds), before adjusting the model to generate simulations under new conditions that cannot be observed in controlled experiments.

The goal of our work was to determine which gait adaptations arise from weakness or contracture of the plantarflexor muscles. To this end, we first created and validated an optimization framework and musculoskeletal model that could generate realistic motions *de novo*. Our controller followed the previously described reflex-based controllers [20,21,23], and the parameters of this controller were iteratively updated within the optimization framework. We validated our results over a wide range of prescribed walking speeds and at self-selected speed; this step was necessary as low gait speed is commonly observed in individuals with gait impairments. We then introduced weakness or contracture in the plantarflexor muscles, generated new gait patterns, and analyzed subsequent changes in the kinematics and kinetics of gait. Our model and results are freely available at https://simtk.org/projects/pfdeficitsgait along with a Docker build file and setup files so others can reproduce our work. We also provide downloads for the control and optimization framework (SCONE, Simulation and CONtrol Environment) and accompanying documentation at http://scone.software to enable others to use and build upon our simulation framework.

Results and Discussion

We generated our simulations using a single shooting method (Fig 1), which is discussed in more detail in the Methods section. We first compare our simulations of unimpaired walking to experimental kinematic, kinetic, and metabolic data. We then detail how we modeled plantarflexor weakness and contracture and discuss the kinematic and kinetic adaptations caused by introducing these deficits into our musculoskeletal model. Video highlights of our results are provided in S1 Video, and videos of all simulations discussed here are provided in S2 Video.

Fig 1. Single shooting framework for dynamic optimization. We trained a planar, musculoskeletal model actuated by 18 Hill-type musculotendon actuators by optimizing the parameters of a gait controller based on an objective function that sought to minimize metabolic cost, avoid falling and injury, and stabilize the head. A gait controller computed muscle excitations, u(t), for a musculoskeletal model to generate a forward simulation. Sensory feedback, based on the model's muscle and joint states, was used in a feedback loop with the gait controller. The objective function quantified the performance of each simulation, and a Covariance Matrix Adaptation Evolutionary Strategy (CMA-ES) optimization method updated the values of the variables in the optimization problem.

Validating the model's gait over a range of speeds

We validated the ability of our model and optimization framework to capture trends in kinematics, kinetics, and spatio-temporal measures when walking at different speeds by generating seven simulations of gait at prescribed speeds between 0.50 m/s and 2.00 m/s, at intervals of 0.25 m/s. All simulations found a steady gait pattern at a speed within 0.05 m/s of the speed prescribed

by the optimization's objective function (S2 Video). Individual comparisons of each speed to experimental data [25] are provided in S1 Fig.

Simulated kinematic and kinetic adaptations, including joint angles, joint moments, and ground reaction forces (GRFs), matched trends observed in experimental data [25] with increasing speeds (Fig 1). Hip and ankle joint angle excursions increased with increasing speeds. Kinetic data, such as peak flexion and extension moments about the hip, knee, and ankle, and the peak horizontal and vertical GRFs, also increased with increasing speeds. Some experimental trends, however, were not captured in our simulations. The knee joint angle range and peak flexion during swing did not increase at higher speeds. At the slowest prescribed speeds (0.50 m/s and 0.75 m/s), the GRFs show a slow resonance not seen in experimental data. This was likely due to our choice for contact parameters, which yielded a softer contact than previous work [22]. While this choice likely contributed to resonance, it also sped simulations up by roughly 2- to 3-fold. We note one aberrant point for the simulation at the slowest speed (0.50 m/s) in the knee joint moment plot that shows a spike of knee extension in early stance, but it does not appear to affect other kinematic or kinetic measures. Overall, while these results show that our simulations capture many salient kinematic and kinetic trends, we must be cautious in interpreting GRF results at speeds at or below 0.75 m/s.

Fig 2. Kinematics and kinetics of simulated walking over a range of speeds. Seven prescribed speeds between 0.50 m/s (blue) and 2.00 m/s (red) at intervals of 0.25 m/s were analyzed. Joint angles (left column) and joint moments (middle column) are plotted for the hip (top row), knee (middle row), and ankle (bottom row). Positive joint angles indicate flexion, and positive joint moments indicate extension. Ground reaction forces (GRFs) (right column) are shown for both

horizontal (top row) and vertical (middle row) directions. With exceptions at the knee joint, we observed trends that occur in experimental data [25], including greater joint angle ranges, joint moments, and ground reaction forces at higher speeds.

Percent stance phase (i.e., the percent of time each foot is in stance during a gait cycle) decreases, and step length and cadence increased with increasing speeds as observed experimentally [25–28] (Fig 2). Percent stance phase was within 2 standard deviations (SD) of experimental data at all speeds. Although the trends of step length and cadence follow experimental data, the simulations generated gaits with a longer step length and a slower cadence than observed experimentally. Our simulations were also able to reproduce experimentally observed trends in metabolic cost of transport over the range of speeds we tested (Fig 2, right panel). In particular, a greater increase in cost of transport was observed when walking slower than optimal as compared to faster than optimal.

Fig 3. Spatio-temporal and metabolic parameters over a range of speeds. Simulated (dots) and experimental (lines) data are plotted for percent stance phase (left), step length (middle left), cadence (middle right), and cost of transport (right). Experimental data for the left three panels are shown with 2 standard deviations [25]. In the right panel, the magnitude and characteristic shape of the cost of transport bowl were similar between the simulated data and experimental data sets [26–28].

Validating self-selected gait of the model

We tested the ability of our model and optimization framework to generate a realistic gait at self-selected speed by generating simulations that did not have a prescribed speed within the

optimization's objective function. Instead, we imposed a minimum speed of 0.75 m/s, which helped guide the optimizer to better solutions but was sufficiently low that it did not affect the final optimized solutions. We generated 3 simulations by initializing the optimization framework with the optimized parameters for 3 of the prescribed speeds from the previous section: slowest (0.50 m/s), middle (1.25 m/s), and fastest (2.00 m/s) speeds. The optimization yielded 3 simulations with similar speeds of 1.23 m/s, 1.21 m/s, and 1.29 m/s, respectively. Each speed was within 2 SDs of the expected self-selected speed (1.25 ± 0.15 m/s) for an individual of our model's leg length [25]. This suggests that our optimization framework can robustly find solutions and is not sensitive to initial guess. For simplicity, only the simulation initialized with the middle speed is described in the remainder of this section.

Our simulated kinematic and kinetic trajectories, including joint angles, joint moments, and GRFs, were similar both in value and shape to experimental data for self-selected gait (Fig 4). For the majority of the gait cycle, simulated trajectories were within 2 SDs of experimental data describing self-selected gait. For each of the trajectories, the root-mean-squared error (RMSE) between simulated and experimental data was no more than 1.55 SD, and for each trajectory except the knee extension moment, the normalized cross-correlation (NCC) [29], which measures shape similarity between the simulated and experimental data sets, was at least 0.82 (Table 1).

Fig 4. Kinematics and kinetics of self-selected gait. Simulated (black line) kinematics and kinetics are compared to experimental data (gray area) [25]. Joint angles (left column) and joint moments (middle column) are plotted for the hip (top row), knee (middle row), and ankle (bottom row). Ground reaction forces (right column) are shown for both horizontal (top row) and vertical (middle row) directions. Positive angles indicate flexion, and positive moments indicate extension.

Note that the experimental data for hip flexion angle was shifted by 11.6° to account for the difference in pelvis orientation definitions between the experimental data set and the musculoskeletal model.

Table 1. Similarity metrics between simulated and experimental data for self-selected gait.

	Angles			**Moments**			**GRFs (stance only)**	
	Hip	**Knee**	**Ankle**	**Hip**	**Knee**	**Ankle**	**Horizontal**	**Vertical**
Root-mean-squared error (SD)	1.55	1.48	0.82	1.08	1.46	1.17	1.04	0.78
Normalized cross-correlation	0.95	0.97	0.82	0.83	-0.04	0.95	0.95	0.99

Root-mean-squared error compares simulation mean trajectories to experimental mean and standard deviation, reported in units of standard deviation (SD). Given the experimental mean and standard deviation over the gait cycle, we compute a Z-score for the simulation data at every 1% of the gait cycle. Then, we take the square root of the sum of squares of all the Z-scores. Normalized cross-correlation compares mean trajectories between simulation and experimental data [25].

The three trajectories with the highest RMSEs, hip joint angle (1.55 SD), knee joint angle (1.48 SD), and knee joint moment (1.46 SD), each contained times when the simulation deviated by more than 2 SDs from the experimental mean. The hip and knee joint angles showed excessive flexion during the swing phase. These were likely compensations due to the simplifications in the model, as degrees of freedom that contributed to foot clearance, such as pelvic list and hip abduction, were not included in the model. Despite the larger RMSEs, the high NCCs of the simulated hip (0.95) and knee (0.97) joint angles to their corresponding experimental trajectories indicate the shape of the simulated and experimental trajectories matched well. The simulated and experimental knee extension moments did not have a similar shape, with a NCC of -0.04. However,

there were large standard deviations in the experimental data during this part of the gait cycle, which is not considered when computing NCC. Differences during early stance explain this discrepancy in knee joint moment trajectories, as the model generated a knee flexion moment when experimental data exhibits a knee extension moment. The model took long steps and landed with an extended knee, causing the GRF to generate a knee extension moment, rather than a knee flexion moment in early stance. Thus, the muscles had to generate a knee flexion moment, rather than a knee extension moment, to prevent hyperextension.

Simulating walking with plantarflexor weakness or contracture

The results of the previous two sections gave us confidence that this model and optimization framework could generate realistic gaits over a wide range of speeds, and could self-select a realistic gait and speed. We then used the framework to study how gait would adapt to deficits in the plantarflexors by adjusting the model's parameters and using the same optimization framework.

We modeled mild, moderate, and severe weakness by reducing a muscle's maximum isometric force (F_o^m) to 25%, 12.5%, and 6.25%, respectively, of its original value. The resulting values for F_o^m were similar to those used in a previous study that computed the minimum plantarflexor muscle strength needed to walk either normally or in a crouch [18]. We modeled mild, moderate, and severe contracture by reducing a muscle's optimal fiber length (l_o^m) to 85%, 70%, and 55%, respectively, of its original value. The severe case was based on experimental data [30] and previously used as a model of contracture [31]. We separately applied each of these 6 deficits to the soleus only (SOL), gastrocnemius only (GAS), or both plantarflexors (PF), to yield 18 total deficit cases.

The optimization framework generated a stable gait in all deficit cases, highlighting its ability to change neural control in response to weakness and contracture (S2 Video). Furthermore, the model's gait was robust to most deficits, and many cases had kinematic and kinetic measures within 2 SDs of walking at a self-selected speed (Fig 5, S2 Fig). By count, the most affected cases were moderate PF weakness, severe PF weakness, severe SOL contracture, and severe PF contracture. In the following sections, we detail the weakness and contracture cases that caused the model to adopt a gait with kinematic or kinetic features outside of 2 SDs of normal walking at a self-selected speed. We provide complete kinematic and kinetic trajectories for all simulations of muscle weakness and contracture in S3 Fig.

Fig 5. Z-scores of key kinematic and kinetic measures of gait for all deficit cases. Z-scores were computed using previous experimental data of individuals walking at a self-selected speed [25]. All 18 cases (dots) are plotted for each measure. A black dot indicates any case within 2 SDs of normal (gray band). A blue or orange dot indicates either a weakness or contracture case, respectively, which is outside of 2 SDs. All of these cases are labeled with the affected muscle or muscles: soleus (SOL), gastrocnemius (GAS), or both (PF); and severity level: mild (Mild), moderate (Mod), or severe (Sev). One other case is labeled (see Peak Plantarflexion Moment, PF Mod*) as it was a clear outlier compared to other deficit cases. The count above each line (e.g., *n = 13*) indicates the number of unlabeled dots.

Walking with plantarflexor weakness

Plantarflexor weakness decreases the capacity of muscles to generate ankle plantarflexion moments, which are critical for generating forward propulsion during walking [1,2,16]. Our

simulations supported this notion as plantarflexion moments during walking were most affected by moderate and severe PF weakness and minimally affected by SOL or GAS weakness only (Fig 5, third row). This suggests that in cases of weakness to only the SOL or GAS, the unimpaired plantarflexor had sufficient capacity to compensate for weakness in the other muscle. For moderate and severe PF weakness, peak ankle plantarflexion moment decreased by 43% and 69%, respectively, when compared to simulated unimpaired walking (Fig 6, bottom row). This highlights the reduced moment generating capacity in these cases.

Fig 6. Ankle kinematics and kinetics for moderate and severe PF weakness. Simulated ankle kinematics and kinetics for unimpaired walking (black lines) and walking with PF weakness (blue lines) are compared to experimental data (gray area) [25]. Ankle dorsiflexion (top) and ankle plantarflexion moment (bottom) are plotted for cases of moderate (left) and severe (right) PF weakness.

Other gait parameters, such as peak horizontal GRF, self-selected walking speed, and percent stance were abnormal for moderate and severe PF weakness as well (Fig 5). Compared to simulated unimpaired walking, peak horizontal GRF decreased by 55% and 70% for moderate and severe PF, respectively, which led to slower walking speeds of 1.01 m/s and 0.87 m/s, respectively. These decreases in gait speed in response to weakness are unsurprising given the direct relationship between the push-off phase and walking speed. Reduced walking speed is commonly observed in individuals with cerebral palsy [32], stroke [33], muscular dystrophy [34], and CMT disease [35], where plantarflexor weakness is common. After accounting for these reduced walking speeds, the model spent an increased percentage of the gait cycle in stance phase, 69% and 74% with moderate

301 and severe PF weakness, respectively. For comparison, simulated unimpaired walking at a slower
302 speed of 0.75 m/s had a percent stance phase of only 63% (Fig 3). These large increases in percent
303 stance phase are consistent with trends seen in the pathological population. For example, CMT
304 patients who had a "plantar flexor strength deficit" were found to adopt a slower gait with an
305 increased time spent in stance phase compared to the gait chosen by patients without the strength
306 deficit [36].

307 Dramatic kinematic compensations at the ankle were observed at the ankle in cases of
308 moderate and severe PF weakness. These models adopted a calcaneal, or "heel-walking", gait,
309 landing with substantially increased ankle dorsiflexion that was maintained throughout stance (Fig
310 6, top row). When compared with simulated unimpaired walking, the model with moderate or
311 severe PF weakness had an increased ankle dorsiflexion at initial contact of 15° and 16°,
312 respectively, and an increased average ankle dorsiflexion during stance of 7° and 11°, respectively.
313 This type of gait is often observed in patients who have received either an intramuscular
314 aponeurotic recession of the plantarflexors or Achilles tendon lengthening to correct contracture
315 [37–39], and it is commonly thought that overlengthening during these procedures can lead to
316 plantarflexor weakness [40,41]. Our simulations support the notion that plantarflexor weakness
317 alone could cause calcaneal gait.

318 While it has been previously hypothesized that plantarflexor weakness may contribute to
319 individuals adopting a crouch gait [18,38,39,41], our simulations did not support this hypothesis.
320 Crouch gait is characterized by increased knee flexion during stance and commonly occurs with
321 increased hip flexion during stance, but our optimization framework found gaits that did not
322 require substantial plantarflexion moment and did not have increased knee and hip flexion during
323 stance (Fig 5, bottom two rows). Our results also differ from previous work that observed a mild

crouch with weakened plantarflexors [21], but a key difference was that our simulations did not have a constrained speed whereas the previous work had a prescribed speed of 1.25 m/s. Although our work does not support the notion that plantarflexor weakness alone will lead to crouch gait, it does not rule out that it could be a contributing factor. For example, it might be that plantarflexor weakness is often associated with weakness and contracture in other muscle groups, and a combination of these deficits along with impaired neural control may lead to crouch gait.

Walking with plantarflexor contracture

Plantarflexor contracture increases passive ankle plantarflexion moments, shifting the ankle's resting position to a more plantarflexed state and limiting ankle range of motion [11,13]. All cases of severe contracture (i.e., SOL, GAS, and PF) had significantly decreased peak values of dorsiflexion in stance (Fig 5, fifth row). One case, mild SOL contracture, appeared to have an opposite effect, but we believe this is an anomaly as the overall ankle position trajectory did not differ much from the unimpaired case (S3D Fig). Models with severe contracture landed on their toes as the ankle was plantarflexed beyond 0° at initial contact, and stayed on their toes throughout stance (Fig 7, top row). Equinus, or "toe-walking," gait is commonly observed in individuals with cerebral palsy [42,43]. Plantarflexor contracture is thought to be a major contributing factor [11,44], and our results support this theory.

Fig 7. Ankle kinematics and kinetics for severe contracture. Simulated ankle kinematics and kinetics for unimpaired walking (black lines) and walking with severe contracture (orange lines) are compared to experimental data (gray area) [25]. Ankle dorsiflexion (top) and ankle

plantarflexion moment (bottom) are plotted for cases of SOL (left), GAS (middle), and PF (right) contracture.

All cases of severe contracture had significantly increased plantarflexion moments during early stance (Fig 7, bottom row), which was expected since an equinus gait necessitates large plantarflexion moments at initial contact to prevent excessive dorsiflexion. In particular, severe SOL or PF contracture had a peak plantarflexion moment during early stance rather than during the push-off phase. Although peak values were largely unaffected, plantarflexion moments during the push-off phase did decrease which led to a subsequent decrease in peak horizontal GRF; all contracture cases had a peak horizontal GRF that was between 2% and 23% lower than our simulated unimpaired case (Fig S2, fourth row).

As severity of contracture increased, models adapted by walking slower and with a shorter stance phase. The three slowest conditions, which included severe SOL, moderate PF, and severe PF contracture, all walked at a significantly slower speed of 1.08 m/s with a slightly smaller percent stance phase of 59% (Fig 5, top two rows). This small decrease in percent stance phase agrees well with experimental data of individuals walking in equinus [45].

In cases of severe SOL, GAS, and PF contracture, the model adopted gaits that were more crouched throughout the whole stance phase, as measured by increased knee and hip flexion, when compared to simulated unimpaired walking (Fig 8). Cases of SOL and PF contracture were more crouched than cases of GAS contracture (S2 Fig, bottom two rows). These results highlight two conclusions. First, contracture in the plantarflexor muscles can lead to dramatic compensations at joints that they do not span. Second, because contracture of only GAS had the smallest effect, our

results suggest that the crouched postures adopted by the model were affected less by the GAS directly flexing the knee and more by walking in equinus.

Fig 8. Hip and knee kinematics for severe contracture. Simulated hip and knee kinematics for unimpaired walking (black lines) and walking with severe contracture (orange lines) are compared to experimental data (gray area) [25]. Hip flexion (top) and knee flexion (bottom) are plotted for cases of SOL (left), GAS (middle), and PF (right) contracture.

Limitations and future work

Simplifications in the model may have affected the observed kinematic trajectories. The model was constrained to sagittal plane motion and consequently lacked degrees of freedom, such as hip abduction, pelvis list, and pelvis rotation, which allow for out-of-plane motions. This made foot clearance more difficult and was likely the cause of compensations in the sagittal plane that increased knee and hip flexion during swing. For the models with deficits, these planar constraints did not allow for commonly observed compensations that are out of the sagittal plane, such as hip circumduction [46,47].

Although we chose to model weakness by decreasing F_o^m and contracture by decreasing l_o^m, there are other ways to model these deficits. For instance, weakness could also be modeled as decreased maximum muscle excitation, which may be important in cases such as stroke [48], and contracture could also be modeled as decreased tendon slack length [49] or increased passive muscle stiffness [50]. These alternate modeling approaches may have led to different gait compensations, and future work to test sensitivity of our results to variations in modeling choices would be valuable.

Although our objective function contained terms that are thought to capture high-level goals of walking, such as minimizing cost of transport [51] while maintaining head stability [52] (see Methods), it may not comprehensively represent goals of human walking, especially amongst individuals with gait pathologies. For example, some individuals may choose a trade-off between metabolic efficiency and joint loading or stability to perturbations. Furthermore, the relative trade-off between these competing objectives likely varies between individuals.

Due to the non-convex nature of the optimization problem and the stochastic nature of our optimizer, the solutions provided here are likely to be local minima rather than global minima. To gain confidence in our solutions, we followed previous work that used multiple optimizations from the same seed and restarted optimizations from the previous best result [23,53], and furthermore, we demonstrated how our solution was robust to different initial seeds (see section on "Validating self-selected gait of the model"). This strategy, however, was computationally expensive, and further work is needed to better search this complex, high-dimensional space. Since a good starting guess can be important for finding reasonable results, we provide our results to assist other researchers in future studies.

Although this work presents a validated framework for studying how isolated changes in muscle parameters may lead to changes in gait, future work on how gait adapts with changes in neural control will further our understanding of pathologic gait. Reflex-based controllers, like the one used here, were useful to ensure that the optimization problem was tractable, but a controller like this cannot predict changes in the underlying control structure. Recent advances in the field of reinforcement learning may be able to generate robust simulations with control patterns that do not have a specified and simplified control structure [54,55].

Conclusion

We present a model and optimization framework suitable for studying sagittal plane adaptations during walking due to muscular deficits. We first validated that, over a wide range of speeds, our model and framework captured many salient features of gait. This framework was then used to study how the model would adapt its gait when plantarflexor weakness or contracture was introduced. Severe plantarflexor weakness caused the model to adopt a calcaneal gait without crouching, while severe plantarflexor contracture caused the model to adopt an equinus gait. Our simulations also showed that contracture of only SOL or both PF caused the model to walk in a more crouched posture than if contracture was applied to only GAS, which suggests that walking in equinus is the major contributor to crouch gait rather than force from the GAS directly flexing the knee. We provide our results freely at https://simtk.org/projects/pfdeficitsgait and software at http://scone.software so that others can easily extend this work.

Methods

Our optimization framework used a single shooting method to solve the dynamic optimization problem of generating a simulation of gait (Fig 1). We implemented our model in OpenSim 3.3 [56,57] and used an optimization and control framework (SCONE) to implement the gait controller, perform the simulation using OpenSim as the plant, and optimize the parameters of our problem.

Musculoskeletal model

The musculoskeletal model (Fig 9) was a planar model based on a previous model used to study the lower limb [58]. The musculoskeletal model had 9 degrees of freedom (dof): a 3-dof

planar joint connected the pelvis to ground; a 1-dof pin joint represented each hip and ankle; and a 1-dof joint with coupled rotation and translation represented each knee. The lumbar joint was locked at 5° of flexion based on previous walking data [2].

Fig 9. A planar musculoskeletal model for walking. The musculoskeletal model had 9 degrees of freedom (dof): the pelvis-to-ground joint was a 3-dof planar joint, each hip and ankle was a 1-dof pin joint, and each knee was a 1-dof coupled joint. The model's 18 musclulotendon actuators (red lines) represented the 9 major uniarticular and biarticular muscle groups per leg that drive sagittal plane motion: iliopsoas (ILPSO), gluteus maximus (GMAX), rectus femoris (RF), biarticular hamstrings (HAMS), vasti (VAS), biceps femoris short head (BFSH), gastrocnemius (GAS), tibialis anterior (TA), and soleus (SOL). A compliant contact model was used to generate forces between the spheres at the heel and toes of the feet and the ground plane.

The model was actuated using eighteen Hill-type muscle-tendon units [59], nine per leg. Muscles with similar functions in the sagittal plane were combined into single muscle-tendon units with combined peak isometric forces to represent 9 major muscle groups per leg: iliopsoas (ILPSO), gluteus maximus (GMAX), rectus femoris (RF), biarticular hamstrings (HAMS), vasti (VAS), biceps femoris short head (BFSH), gastrocnemius (GAS), tibialis anterior (TA), and soleus (SOL). Peak isometric forces were based on a previous musculoskeletal model [60], whose muscle volumes were based on young, healthy subjects [3]. The tendon strain at peak isometric force was 4.9% [60,61] for all muscles except for the plantarflexors, whose values were set to 10% [62]. To better match passive muscle forces during walking [63], we adjusted the passive force-length curves of the HAMS, VAS, and RF to decrease their passive forces (S1 Table). The tendon slack

length of each muscle was calculated based on experimental data [64], as done previously in other musculoskeletal models [60,65]. We set maximum muscle fiber contraction velocity to 15 l_o^m/s [62,66]. All muscle-tendon parameters are summarized in S1 Table.

Ligaments were modeled as nonlinear, rotational springs that generated torques when a joint was hyperflexed or hyperextended. In our model, ligaments generated torques when the hip was flexed beyond 120° or extended beyond 30°; the knee was flexed beyond 140° or extended beyond 0°; and the ankle was dorsiflexed beyond 20° or plantarflexed beyond 40°.

A compliant contact model [67,68] was used to generate forces between the feet and the ground. Each foot had three contact spheres: one sphere with a radius of 5 cm represented the heel, and two spheres, each with a radius of 2.5cm, represented the toes. All contact spheres had the following parameters: stiffness coefficient of 500,000 $N/m^{3/2}$, dissipation coefficient of 1.0 s/m, static and dynamic friction coefficients of 0.8, viscous friction coefficient of 0, and transition velocity of 0.1 m/s.

As described in the Results and Discussion, we introduced two types of deficits into the musculoskeletal model: weakness and contracture. We modeled mild, moderate, and severe weakness by reducing the peak isometric force of a muscle (F_o^m) by 25%, 12.5%, and 6.25%, respectively, of the value in the unimpaired model. We modeled mild, moderate, and severe contracture by reducing the optimal fiber length of a muscle (l_o^m) by 85%, 70%, and 55%, respectively, of the value in the unimpaired model. All 6 of these muscle deficits were applied to the SOL, the GAS, or both the SOL and GAS, for a total of 18 cases.

Gait controller

The gait controller was based on previous reflex-based controllers for human locomotion [20,21,23] and used a combination of a high-level state machine and low-level control laws to calculate muscle excitations. Our controller had 5 high-level states that represented key points in the gait cycle for each leg: early stance (ES), mid-stance (MS), pre-swing (PS), swing (S), and landing preparation (LP). Of the 5 transitions between these high-level states, transitions between 4 of the states were controlled by 4 thresholds that were free parameters in the optimization: 1) ES to MS: horizontal distance between the ipsilateral foot and pelvis was lower than a threshold; 2) PS to S: GRF on the ipsilateral foot was lower than a threshold; 3) S to LP: horizontal distance between the ipsilateral foot and pelvis was greater than a threshold; and 4) LP to ES: GRF on ipsilateral foot was greater than a threshold. The fifth transition, MS to PS, was not controlled by a free parameter and occurred when the contralateral leg entered ES state.

Low-level control laws were active or inactive depending on the high-level controller (Fig 10). There were 5 types of control laws: constant (C), length feedback (L), velocity feedback (V), force feedback (F), and proportional-derivative (PD). All muscle-based feedback laws were positive feedback (i.e., L+, V+, F+) onto the same muscle, except for a negative force feedback (F-) from the soleus to the tibialis anterior. PD control was only used to control the pelvis tilt angle (θ) and velocity ($\dot{\theta}$) with respect to ground using the muscles crossing the hip joint (i.e., ILPSO, GMAX, and HAMS). Excitations (u) are calculated over time (t) by the following equations:

$$u_C = K_C \tag{1}$$

$$u_{L+} = \max\left(0, K_{L+}\left[l(t - t_D) - l_o\right]\right) \tag{2}$$

$$u_{V+} = \max\left(0, K_{V+}\left[v(t - t_D)\right]\right) \tag{3}$$

$$u_{F\pm} = \pm K_{F\pm} F(t - t_D) \tag{4}$$

$$u_{PD} = K_p\left[\theta(t - t_D) - \theta_o\right] + K_v\left[\dot{\theta}(t - t_D)\right] \tag{5}$$

States calculated from the model were muscle length (l), muscle velocity (v), muscle force (F), and pelvis tilt orientation (θ) and velocity ($\dot{\theta}$). In total, there were 70 free parameters of the optimization, including the controller gains (K_C, K_{L+}, K_{V+}, $K_{F\pm}$, K_p, and K_v), and offsets for muscle length feedback (l_o) and proportional feedback of θ (θ_o). For all positive feedback and PD control laws, the parameter for time delay, t_D, was set for each muscle depending on the most proximal joint over which the muscle crosses: t_D was 5 ms for the hip, 10 ms for the knee, and 20 ms for the ankle [20]. For the F- law from the soleus to the tibialis anterior, t_D was 40 ms. When considered with a first-order activation time constant of 10 ms, this delay better represented the short-latency TA suppression (56 to 74 ms) observed in experiments [69]. Overall, however, the delays used were still shorter than those measured experimentally [70].

Fig 10. The gait controller used a combination of a state machine and low-level control laws to determine excitations. The state machine had three states in stance (i.e., early stance (ES), mid-stance (MS), and pre-swing (PS)) and two states in swing (i.e., swing (S) and landing preparation (LP)), and it determined when low-level control laws were active. Low-level control laws included constant signals (C) and feedback terms based on muscle length (L), muscle velocity (V), muscle force (F), and proportional-derivative control (PD) based on the pelvis tilt angle. Positive and negative feedback are denoted by (+) and (-), respectively. All feedback laws based on muscle states acted upon the same muscle, except for a negative force feedback from the soleus to the tibialis anterior.

Simulation and optimization framework

OpenSim was used to form the model's equations of motion and integrate them [56,57]. The state of the model was initialized by first setting the pelvis's horizontal position to 0 m. Then, we set initial angular positions and velocities, and the speed of the pelvis according to free parameters in the optimization. Although optimizing velocities may add extra energy into the system, we do not think this affected our results as we found step-to-step variability to be small, and we only analyzed kinematics and kinetics after the first two steps taken. Finally, the vertical position of the pelvis was set such that the GRF was equal to half of the model's body weight. Integration continued until the desired simulation time was reached or until the model fell, which we defined as the model's center of mass (COM) height falling below 0.8 times the height of the COM at the start of the simulation.

To evaluate a set of design parameters, we defined an objective function, J, which we sought to minimize. The objective, J, quantified high-level tasks of walking:

$$J = J_{\text{cot}} + w_{\text{spd}} J_{\text{spd}} + w_{\text{inj}} J_{\text{inj}} + w_{\text{head}} J_{\text{head}} \tag{6}$$

The goal was to minimize the gross cost of transport (J_{cot}) while maintaining a prescribed step-to-step speed within a range, avoiding falling (J_{spd}), avoiding ligament injury (J_{inj}), and stabilizing the head (J_{head}). To balance competing objectives, the weights were manually adjusted to the following: $w_{\text{spd}} = 10{,}000$, $w_{\text{inj}} = 0.1$, and $w_{\text{head}} = 0.25$. These weights emphasized finding a gait that did not fall over one that minimized cost of transport, injury, and accelerations at the head. For optimized solutions, the contribution from the J_{head} term was larger than those from the J_{spd} and J_{inj} terms, and thus our results were most sensitive to our choice of w_{head}. Because of this, our choice for w_{head} represents a trade-off between head stability, especially during early stance, and cost of transport.

J_{cot} penalized simulations in which the model walked in a less metabolically efficient manner [51] and was calculated by summing the basal and per-muscle metabolic rates [71,72] to estimate the gross metabolic rate ($\dot{E}$) over the duration of the simulation (t_{end}), and normalizing by the mass of the model (m) and distance travelled (d):

$$J_{\text{cot}} = \frac{\int_0^{t_{\text{end}}} \dot{E} dt}{md} \tag{7}$$

J_{spd} penalized simulations in which the model fell at a time (t_{fall}) before the desired simulation end time (t_{des}) and had step speeds outside of a prescribed range. J_{spd} was calculated using the following equations:

$$J_{\text{spd}} = 1 - \sum_s \frac{t_s v_{s,\text{pen}}}{v_{\text{min}}} \tag{8}$$

$$v_{s,\text{pen}} = \begin{cases} 0, & t_{\text{end}} = t_{\text{fall}} \\ \max\left[0, 1 - \phi(v_s, v_{\text{min}}, v_{\text{max}})\right], & t_{\text{end}} = t_{\text{des}} \end{cases} \tag{9}$$

$$\phi(\varphi, \varphi_{\text{min}}, \varphi_{\text{max}}) = \begin{cases} 0, & \varphi_{\text{min}} < \varphi < \varphi_{\text{max}} \\ \varphi_{\text{min}} - \varphi, & \varphi < \varphi_{\text{min}} \\ \varphi - \varphi_{\text{max}}, & \varphi > \varphi_{\text{max}} \end{cases} \tag{10}$$

where s denotes a step, t_s is the duration of a step, $v_{s,\text{pen}}$ is a penalty for a given step (ranging between 0 and 1, where 1 is no penalty), v_s is the step speed, v_{min} and v_{max} define the minimum and maximum speeds allowed without a penalty, and Φ applies a linear penalty if v_s is not between v_{min} and v_{max}. If all steps were within the speed range, J_{spd} was 0, and if the model immediately fell, J_{spd} was 1. For any given step in which the speed was outside of the range, the step was linearly penalized more heavily (i.e., $v_{s,\text{pen}}$ was closer to 0) the further the speed was out of the range, and its final contribution to J_{spd} was scaled by t_{s}. For simulations with a prescribed speed, the speed range was ±0.05 m/s of the prescribed speed. For example, to prescribe a speed of 1.25 m/s, v_{min} = 1.20 m/s and v_{max} = 1.30 m/s. For simulations without a prescribed speed, v_{min} was 0.75 m/s, and v_{max} was arbitrarily large.

570 J_{inj} penalized simulations in which the model engaged the ligaments and was calculated by
571 integrating the sum of joint torques (T_j) squared generated by the model's ligaments:

572 $$J_{\text{inj}} = \int_0^{t_{\text{end}}} \sum_j T_j^2 dt \quad (11)$$

573 Since head stability is commonly regarded as an important task during gait [73], J_{head}
574 penalized simulations in which the model had excessively large accelerations and was calculated
575 by the following equation and Eq 10:

576 $$J_{\text{head}} = \int_0^{t_{\text{end}}} \left[\phi(a_x, a_{x,\min}, a_{x,\max})^2 + \phi(a_y, a_{y,\min}, a_{y,\max})^2\right] dt \quad (12)$$

577 where a_x and a_y are the horizontal and vertical accelerations at a point located near the center of
578 the head, and $a_{x,\min}$, $a_{x,\max}$, $a_{y,\min}$, and $a_{y,\max}$ determine the bounds between which no penalty is
579 applied if a_x and a_y are within the bounds. We set our acceleration bounds as $a_{x,\min} = -0.25g$, $a_{x,\max}$
580 $= 0.25g$, $a_{y,\min} = -0.50g$, and $a_{y,\max} = 0.50g$, which we approximated from experimental data of
581 human walking [52].

582 To solve our optimization problem, we used an evolutionary strategy called Covariance
583 Matrix Adaptation Evolutionary Strategy (CMA-ES) with a rank-μ update [74]. In total, there were
584 90 design variables: 74 for the gains, offsets, and transition parameters in the gait controller, and
585 16 for the parameters that set the model's initial state. We set the CMA-ES parameters such that
586 the population size of each generation (λ) was 16 and the update step for each generation used only
587 the 8 best solutions (μ). Because these types of problems tend to have noisy, non-convex search
588 spaces, and CMA-ES is a stochastic algorithm, we ran a set of multiple parallel optimizations with
589 the same initial guess, and used the best solution from the set to seed the next set of optimizations
590 as has been done previously [23,53]. Refer to S2 Table for the initial standard deviations used for
591 each parameter. We chose to stop when the best solution from a set had an objective function value

that was no better than 5% of the one from the previous set, as we observed optimized solutions that were within 5% of each other were qualitatively similar.

Generating simulations of gait

To generate simulations of gait with a prescribed speed, we used 10 second simulations (t_{des} = 10 s) and a set of 20 parallel optimizations, each with a maximum of 3000 generations for CMA-ES. There were 7 simulations that were generated at prescribed speeds between 0.50 m/s and 2.00 m/s at an interval of 0.25 m/s. We first trained the model at the middle speed, 1.25 m/s, and then used those results to seed the neighboring speeds, continuing until we reached the lowest and highest speeds. For example, the solution for our 1.25 m/s case was used to seed the 1.00 m/s case, which was then used to seed the 0.75 m/s case.

To generate simulations of gait with a self-selected speed, we used longer, 30 second simulations (t_{des} = 30 s), as we found that solutions with a shorter desired simulation time would systematically fall forward at the end without a tight bound on step speed. We used a set of 10 parallel optimizations, each with a maximum of 1500 generations for CMA-ES. We generated 3 simulations of unimpaired gait at a self-selected speed, seeding from solutions of the slowest (0.50 m/s), middle (1.25 m/s), and fastest (2.00 m/s) cases from above. We also generated 18 simulations of impaired gait, starting with the unimpaired solution and seeding the next more severe case. For example, the solution from the unimpaired case was used to seed the mild SOL weakness case, which was used to seed the moderate case, which was finally used to seed the severe case.

Acknowledgments

We would like to thank Apoorva Rajagopal and Jennifer Yong for their insightful feedback on this manuscript, and Christopher Dembia, Shrinidhi Lakshmikanth, Ajay Seth, and Thomas Uchida for helpful technical discussions. We thank the Stanford Research Computing Center for providing computational resources and support that contributed to these research results.

References

1. Neptune RR, Kautz SA, Zajac FE. Contributions of the individual ankle plantar flexors to support, forward progression and swing initiation during walking. J Biomech. 2001;34: 1387–1398. doi:10.1016/S0021-9290(01)00105-1

2. Liu MQ, Anderson FC, Schwartz MH, Delp SL. Muscle contributions to support and progression over a range of walking speeds. J Biomech. 2008;41: 3243–3252. doi:10.1016/j.jbiomech.2008.07.031

3. Handsfield GG, Meyer CH, Abel MF, Blemker SS. Heterogeneity of muscle sizes in the lower limbs of children with cerebral palsy. Muscle Nerve. 2016;53: 933–945. doi:10.1002/mus.24972

4. Noble JJ, Fry NR, Lewis AP, Keevil SF, Gough M, Shortland AP. Lower limb muscle volumes in bilateral spastic cerebral palsy. Brain Dev. 2014;36: 294–300. doi:10.1016/J.BRAINDEV.2013.05.008

5. Barber L, Hastings-Ison T, Baker R, Barrett R, Lichtwark G. Medial gastrocnemius muscle volume and fascicle length in children aged 2 to 5 years with cerebral palsy. Dev Med Child Neurol. 2011;53: 543–548. doi:10.1111/j.1469-8749.2011.03913.x

6. Kim CM, Eng JJ. The Relationship of Lower-Extremity Muscle Torque to Locomotor

636 Performance in People With Stroke. Phys Ther. 2003;83: 49–57. doi:10.1093/ptj/83.1.49

637 7. Hoogerwaard EM, Bakker E, Ippel PF, Oosterwijk JC, Majoor-Krakauer DF, Leschot NJ,
638 et al. Signs and symptoms of Duchenne muscular dystrophy and Becker muscular
639 dystrophy among carriers in The Netherlands: a cohort study. Lancet. 1999;353: 2116—
640 2119. doi:10.1016/s0140-6736(98)10028-4

641 8. Bushby K, Finkel R, Birnkrant DJ, Case LE, Clemens PR, Cripe L, et al. Diagnosis and
642 management of Duchenne muscular dystrophy, part 1: diagnosis, and pharmacological and
643 psychosocial management. Lancet Neurol. 2010;9: 77–93. doi:10.1016/S1474-
644 4422(09)70271-6

645 9. Sabir M, Lyttle D. Pathogenesis of pes cavus in Charcot-Marie-Tooth disease. Clin
646 Orthop Relat Res. 1983; 173—178.

647 10. Barber L, Barrett R, Lichtwark G. Passive muscle mechanical properties of the medial
648 gastrocnemius in young adults with spastic cerebral palsy. J Biomech. 2011;44: 2496–
649 2500. doi:10.1016/j.jbiomech.2011.06.008

650 11. Mathewson MA, Ward SR, Chambers HG, Lieber RL. High resolution muscle
651 measurements provide insights into equinus contractures in patients with cerebral palsy. J
652 Orthop Res. 2015;33: 33–39. doi:10.1002/jor.22728

653 12. Lin P-Y, Yang Y-R, Cheng S-J, Wang R-Y. The Relation Between Ankle Impairments
654 and Gait Velocity and Symmetry in People With Stroke. Arch Phys Med Rehabil.
655 2006;87: 562–568. doi:10.1016/J.APMR.2005.12.042

656 13. Gao F, Grant TH, Roth EJ, Zhang L-Q. Changes in Passive Mechanical Properties of the
657 Gastrocnemius Muscle at the Muscle Fascicle and Joint Levels in Stroke Survivors. Arch

Phys Med Rehabil. 2009;90: 819–826. doi:10.1016/J.APMR.2008.11.004

14. Mercuri E, Bushby K, Ricci E, Birchall D, Pane M, Kinali M, et al. Muscle MRI findings in patients with limb girdle muscular dystrophy with calpain 3 deficiency (LGMD2A) and early contractures. Neuromuscul Disord. 2005;15: 164–171. doi:10.1016/J.NMD.2004.10.008

15. Bushby K, Finkel R, Birnkrant DJ, Case LE, Clemens PR, Cripe L, et al. Diagnosis and management of Duchenne muscular dystrophy, part 2: implementation of multidisciplinary care. Lancet Neurol. 2010;9: 177–189. doi:https://doi.org/10.1016/S1474-4422(09)70272-8

16. Sutherland DH, Cooper L, Daniel D. The role of the ankle plantar flexors in normal walking. JBJS. 1980;62.

17. Steele KM, Seth A, Hicks JL, Schwartz MS, Delp SL. Muscle contributions to support and progression during single-limb stance in crouch gait. J Biomech. 2010;43: 2099–2105. doi:10.1016/J.JBIOMECH.2010.04.003

18. Steele KM, van der Krogt MM, Schwartz MH, Delp SL. How much muscle strength is required to walk in a crouch gait? J Biomech. 2012;45: 2564–2569. doi:10.1016/J.JBIOMECH.2012.07.028

19. van der Krogt MM, Bar-On L, Kindt T, Desloovere K, Harlaar J. Neuro-musculoskeletal simulation of instrumented contracture and spasticity assessment in children with cerebral palsy. J Neuroeng Rehabil. 2016;13: 64. doi:10.1186/s12984-016-0170-5

20. Geyer H, Herr H. A Muscle-Reflex Model That Encodes Principles of Legged Mechanics Produces Human Walking Dynamics and Muscle Activities. IEEE Trans Neural Syst

680 Rehabil Eng. 2010;18: 263–273. doi:10.1109/TNSRE.2010.2047592

681 21. Wang JM, Hamner SR, Delp SL, Koltun V. Optimizing Locomotion Controllers Using
682 Biologically-Based Actuators and Objectives. ACM Trans Graph. 2012;31: 25.
683 doi:10.1145/2185520.2185521

684 22. Dorn TW, Wang JM, Hicks JL, Delp SL. Predictive Simulation Generates Human
685 Adaptations during Loaded and Inclined Walking. PLoS One. 2015;10: e0121407.
686 doi:10.1371/journal.pone.0121407

687 23. Song S, Geyer H. A neural circuitry that emphasizes spinal feedback generates diverse
688 behaviours of human locomotion. J Physiol. 2015;593: 3493–3511. doi:10.1113/JP270228

689 24. Song S, Geyer H. Predictive neuromechanical simulations indicate why walking
690 performance declines with ageing. J Physiol. 2018;596: 1199–1210.
691 doi:10.1113/JP275166

692 25. Schwartz MH, Rozumalski A, Trost JP. The effect of walking speed on the gait of
693 typically developing children. J Biomech. 2008;41: 1639–1650.
694 doi:10.1016/j.jbiomech.2008.03.015

695 26. Ralston HJ. Energy-speed relation and optimal speed during level walking. Int Zeitschrift
696 für Angew Physiol einschließlich Arbeitsphysiologie. 1958;17: 277–283.
697 doi:10.1007/BF00698754

698 27. Martin PE, Rothstein DE, Larish DD. Effects of age and physical activity status on the
699 speed-aerobic demand relationship of walking. J Appl Physiol. 1992;73: 200–206.
700 doi:10.1152/jappl.1992.73.1.200

701 28. Browning RC, Baker EA, Herron JA, Kram R. Effects of obesity and sex on the energetic

702 cost and preferred speed of walking. J Appl Physiol. 2006;100: 390–398.
703 doi:10.1152/japplphysiol.00767.2005

704 29. Wren TAL, Do KP, Rethlefsen SA, Healy B. Cross-correlation as a method for comparing
705 dynamic electromyography signals during gait. J Biomech. 2006;39: 2714–2718.
706 doi:10.1016/J.JBIOMECH.2005.09.006

707 30. Ziv I, Blackburn N, Rang M, Koreska J. Muscle growth in normal and spastic mice. Dev
708 Med Child Neurol. 1984;26: 94–99. doi:10.1111/j.1469-8749.1984.tb04412.x

709 31. Delp SL, Statler K, Carroll NC. Preserving plantar flexion strength after surgical treatment
710 for contracture of the triceps surae: A computer simulation study. J Orthop Res. 1995;13:
711 96–104. doi:10.1002/jor.1100130115

712 32. Abel MF, Damiano DL. Strategies for increasing walking speed in diplegic cerebral palsy.
713 J Pediatr Orthop. 1996;16: 753—758. doi:10.1097/00004694-199611000-00010

714 33. Turnbull GI, Charteris J, Wall JC. A comparison of the range of walking speeds between
715 normal and hemiplegic subjects. Scand J Rehabil Med. 1995;27: 175—182.

716 34. Khodadadeh S, McClelland MR, Patrick JH. Variations of Gait Parameters in Duchenne
717 Muscular Dystrophy. Proc Inst Mech Eng Part H J Eng Med. 1990;204: 241–243.
718 doi:10.1243/PIME_PROC_1990_204_262_02

719 35. Newman CJ, Walsh M, O'Sullivan R, Jenkinson A, Bennett D, Lynch B, et al. The
720 characteristics of gait in Charcot-Marie-Tooth disease types I and II. Gait Posture.
721 2007;26: 120–127. doi:10.1016/J.GAITPOST.2006.08.006

722 36. Don R, Serrao M, Vinci P, Ranavolo A, Cacchio A, Ioppolo F, et al. Foot drop and plantar
723 flexion failure determine different gait strategies in Charcot-Marie-Tooth patients. Clin

724 Biomech. 2007;22: 905–916. doi:10.1016/J.CLINBIOMECH.2007.06.002

725 37. Dreher T, Buccoliero T, Wolf SI, Heitzmann D, Gantz S, Braatz F, et al. Long-term
726 results after gastrocnemius-soleus intramuscular aponeurotic recession as a part of
727 multilevel surgery in spastic diplegic cerebral palsy. J Bone Joint Surg Am. 2012;94:
728 627—637. doi:10.2106/jbjs.k.00096

729 38. Dietz FR, Albright JC, Dolan L. Medium-term follow-up of Achilles tendon lengthening
730 in the treatment of ankle equinus in cerebral palsy. Iowa Orthop J. 2006;26: 27–32.

731 39. Segal LS, Thomas SE, Mazur JM, Mauterer M. Calcaneal gait in spastic diplegia after
732 heel cord lengthening: a study with gait analysis. J Pediatr Orthop. 1989;9: 697—701.

733 40. Garbarino JL, Clancy M. A geometric method of calculating tendo Achillis lengthening. J
734 Pediatr Orthop. 1985;5: 573—576.

735 41. Gage JR. Surgical treatment of knee dysfunction in cerebral palsy. Clin Orthop Relat Res.
736 1990; 45—54.

737 42. Fulford GE. Surgical management of ankle and foot deformities in cerebral palsy. Clin
738 Orthop Relat Res. 1990; 55—61.

739 43. Wren TAL, Rethlefsen S, Kay RM. Prevalence of specific gait abnormalities in children
740 with cerebral palsy: influence of cerebral palsy subtype, age, and previous surgery. J
741 Pediatr Orthop. 2005;25: 79—83. doi:10.1097/00004694-200501000-00018

742 44. Wren TAL, Do KP, Kay RM. Gastrocnemius and soleus lengths in cerebral palsy equinus
743 gait—differences between children with and without static contracture and effects of
744 gastrocnemius recession. J Biomech. 2004;37: 1321–1327.
745 doi:10.1016/J.JBIOMECH.2003.12.035

746 45. Perry J, Burnfield JM. Gait Analysis: Normal and pathological function. 2010. SLACK
747 Inc. : 85–534.

748 46. Gage JR, Novacheck TF. An update on the treatment of gait problems in cerebral palsy. J
749 Pediatr Orthop B. 2001;10: 265—274. doi:10.1097/00009957-200110000-00001

750 47. Kim CM, Eng JJ. Magnitude and pattern of 3D kinematic and kinetic gait profiles in
751 persons with stroke: relationship to walking speed. Gait Posture. 2004;20: 140–146.
752 doi:10.1016/J.GAITPOST.2003.07.002

753 48. Newham DJ, Hsiao SF. Knee muscle isometric strength, voluntary activation and
754 antagonist co-contraction in the first six months after stroke. Disabil Rehabil. 2001;23:
755 379—386. doi:10.1080/0963828001006656

756 49. Herbert RD, Crosbie J. Rest length and compliance of non-immobilised and immobilised
757 rabbit soleus muscle and tendon. Eur J Appl Physiol Occup Physiol. 1997;76: 472–479.
758 doi:10.1007/s004210050277

759 50. Smith LR, Lee KS, Ward SR, Chambers HG, Lieber RL. Hamstring contractures in
760 children with spastic cerebral palsy result from a stiffer extracellular matrix and increased
761 in vivo sarcomere length. J Physiol. 2011;589: 2625–2639.
762 doi:10.1113/jphysiol.2010.203364

763 51. Selinger JC, O'Connor SM, Wong JD, Donelan JM. Humans Can Continuously Optimize
764 Energetic Cost during Walking. Curr Biol. 2015;25: 2452–2456.
765 doi:10.1016/J.CUB.2015.08.016

766 52. Menz HB, Lord SR, Fitzpatrick RC. Acceleration patterns of the head and pelvis when
767 walking on level and irregular surfaces. Gait Posture. 2003;18: 35–46. doi:10.1016/S0966-

6362(02)00159-5

53. Ong CF, Hicks JL, Delp SL. Simulation-Based Design for Wearable Robotic Systems: An Optimization Framework for Enhancing a Standing Long Jump. IEEE Trans Biomed Eng. 2016;63: 894–903. doi:10.1109/TBME.2015.2463077

54. Heess N, TB D, Sriram S, Lemmon J, Merel J, Wayne G, et al. Emergence of Locomotion Behaviours in Rich Environments. 2017; Available: arxiv:1707.02286

55. Kidziński Ł, Mohanty SP, Ong CF, Hicks JL, Carroll SF, Levine S, et al. Learning to Run Challenge: Synthesizing Physiologically Accurate Motion Using Deep Reinforcement Learning. In: Escalera S, Weimer M, editors. The NIPS ’17 Competition: Building Intelligent Systems. Cham: Springer International Publishing; 2018. pp. 101–120.

56. Delp SL, Anderson FC, Arnold AS, Loan P, Habib A, John CT, et al. OpenSim: open-source software to create and analyze dynamic simulations of movement. IEEE Trans Biomed Eng. 2007;54: 1940—1950. doi:10.1109/tbme.2007.901024

57. Seth A, Hicks JL, Uchida TK, Habib A, Dembia CL, Dunne JJ, et al. OpenSim: Simulating musculoskeletal dynamics and neuromuscular control to study human and animal movement. PLOS Comput Biol. 2018;14: 1–20. doi:10.1371/journal.pcbi.1006223

58. Delp SL, Loan JP, Hoy MG, Zajac FE, Topp EL, Rosen JM. An interactive graphics-based model of the lower extremity to study orthopaedic surgical procedures. IEEE Trans Biomed Eng. 1990;37: 757–767. doi:10.1109/10.102791

59. Thelen DG. Adjustment of Muscle Mechanics Model Parameters to Simulate Dynamic Contractions in Older Adults. J Biomech Eng. 2003;125: 70–77. doi:10.1115/1.1531112

60. Rajagopal A, Dembia CL, DeMers MS, Delp DD, Hicks JL, Delp SL. Full-Body

Musculoskeletal Model for Muscle-Driven Simulation of Human Gait. IEEE Trans Biomed Eng. 2016;63: 2068–2079. doi:10.1109/TBME.2016.2586891

61. Millard M, Uchida T, Seth A, Delp SL. Flexing Computational Muscle: Modeling and Simulation of Musculotendon Dynamics. J Biomech Eng. 2013;135: 21005–21011. doi:10.1115/1.4023390

62. Arnold EM, Hamner SR, Seth A, Millard M, Delp SL. How muscle fiber lengths and velocities affect muscle force generation as humans walk and run at different speeds. J Exp Biol. 2013; doi:10.1242/jeb.075697

63. Whittington B, Silder A, Heiderscheit B, Thelen DG. The contribution of passive-elastic mechanisms to lower extremity joint kinetics during human walking. Gait Posture. 2008;27: 628–634. doi:10.1016/J.GAITPOST.2007.08.005

64. Ward SR, Eng CM, Smallwood LH, Lieber RL. Are Current Measurements of Lower Extremity Muscle Architecture Accurate? Clin Orthop Relat Res. 2009;467: 1074–1082. doi:10.1007/s11999-008-0594-8

65. Arnold EM, Ward SR, Lieber RL, Delp SL. A Model of the Lower Limb for Analysis of Human Movement. Ann Biomed Eng. 2010;38: 269–279. doi:10.1007/s10439-009-9852-5

66. Thelen DG, Chumanov ES, Best TM, Swanson SC, Heiderscheit BC. Simulation of biceps femoris musculotendon mechanics during the swing phase of sprinting. Med Sci Sports Exerc. 2005;37: 1931—1938. doi:10.1249/01.mss.0000176674.42929.de

67. Hunt KH, Crossley FRE. Coefficient of Restitution Interpreted as Damping in Vibroimpact. J Appl Mech. 1975;42: 440–445. doi:10.1115/1.3423596

68. Sherman MA, Seth A, Delp SL. Simbody: multibody dynamics for biomedical research.

Procedia IUTAM. 2011;2: 241–261. doi:10.1016/J.PIUTAM.2011.04.023

69. Duysens J, Trippel M, Horstmann GA, Dietz V. Gating and reversal of reflexes in ankle muscles during human walking. Exp Brain Res. 1990;82: 351–358. doi:10.1007/BF00231254

70. Frijns CJM, Laman DM, van Duijn MAJ, van Duijn H. Normal values of patellar and ankle tendon reflex latencies. Clin Neurol Neurosurg. 1997;99: 31–36. doi:10.1016/S0303-8467(96)00593-8

71. Umberger BR, Gerritsen KGM, Martin PE. A model of human muscle energy expenditure. Comput Methods Biomech Biomed Engin. 2003;6: 99—111. doi:10.1080/1025584031000091678

72. Uchida TK, Hicks JL, Dembia CL, Delp SL. Stretching Your Energetic Budget: How Tendon Compliance Affects the Metabolic Cost of Running. PLoS One. 2016;11: 1–19. doi:10.1371/journal.pone.0150378

73. Bril B, Ledebt A. Head Coordination as a Means to Assist Sensory Integration in Learning to Walk. Neurosci Biobehav Rev. 1998;22: 555–563. doi:10.1016/S0149-7634(97)00044-4

74. Hansen N, Kern S. Evaluating the CMA Evolution Strategy on Multimodal Test Functions. In: Yao X, Burke EK, Lozano JA, Smith J, Merelo-Guervós JJ, Bullinaria JA, et al., editors. Parallel Problem Solving from Nature - PPSN VIII. Berlin, Heidelberg: Springer Berlin Heidelberg; 2004. pp. 282–291.

Supporting information

S1A Fig. Simulated walking at 0.55 m/s vs experimental data at 0.50 ± 0.20 m/s. To facilitate comparison, normalized speed from experimental data was converted using the model's leg length (0.856 m).

S1B Fig. Simulated walking at 0.79 m/s vs experimental data at 0.84 ± 0.16 m/s. To facilitate comparison, normalized speed from experimental data was converted using the model's leg length (0.856 m).

S1C Fig. Simulated walking at 1.04 m/s vs experimental data at 0.84 ± 0.16 m/s. To facilitate comparison, normalized speed from experimental data was converted using the model's leg length (0.856 m).

S1D Fig. Simulated walking at 1.22 m/s vs experimental data at 1.24 ± 0.15 m/s. To facilitate comparison, normalized speed from experimental data was converted using the model's leg length (0.856 m).

S1E Fig. Simulated walking at 1.46 m/s vs experimental data at 1.62 ± 0.18 m/s. To facilitate comparison, normalized speed from experimental data was converted using the model's leg length (0.856 m).

S1F Fig. Simulated walking at 1.71 m/s vs experimental data at 1.62 ± 0.18 m/s. To facilitate comparison, normalized speed from experimental data was converted using the model's leg length (0.856 m).

S1G Fig. Simulated walking at 1.96 m/s vs experimental data at 2.01 ± 0.27 m/s. To facilitate comparison, normalized speed from experimental data was converted using the model's leg length (0.856 m).

S2 Fig. Key kinematic and kinetic parameters for all deficits. This plot accompanies Fig 5 and shows key parameters for walking with simulated weakness (blue) and contracture (orange) of the SOL, GAS, or both (PF) along with simulated healthy gait (dotted line). Increasing color intensity indicates increasing deficit severity.

S3A Fig. Simulated walking with mild, moderate, and severe soleus (SOL) weakness.

S3B Fig. Simulated walking with mild, moderate, and severe gastrocnemius (GAS) weakness.

S3C Fig. Simulated walking with mild, moderate, and severe soleus and gastrocnemius (PF) weakness.

S3D Fig. Simulated walking with mild, moderate, and severe soleus (SOL) contracture.

S3E Fig. Simulated walking with mild, moderate, and severe gastrocnemius (GAS) contracture.

S3F Fig. Simulated walking with mild, moderate, and severe soleus and gastrocnemius (PF) contracture.

S1 Table. Muscle parameters for the unimpaired musculoskeletal model.

S2 Table. Initial Covariance Matrix Adaptation Evolutionary Strategy (CMA-ES) standard deviation for each free parameter.

S1 Video. Highlights.

S2 Video. Compilation of all simulations.

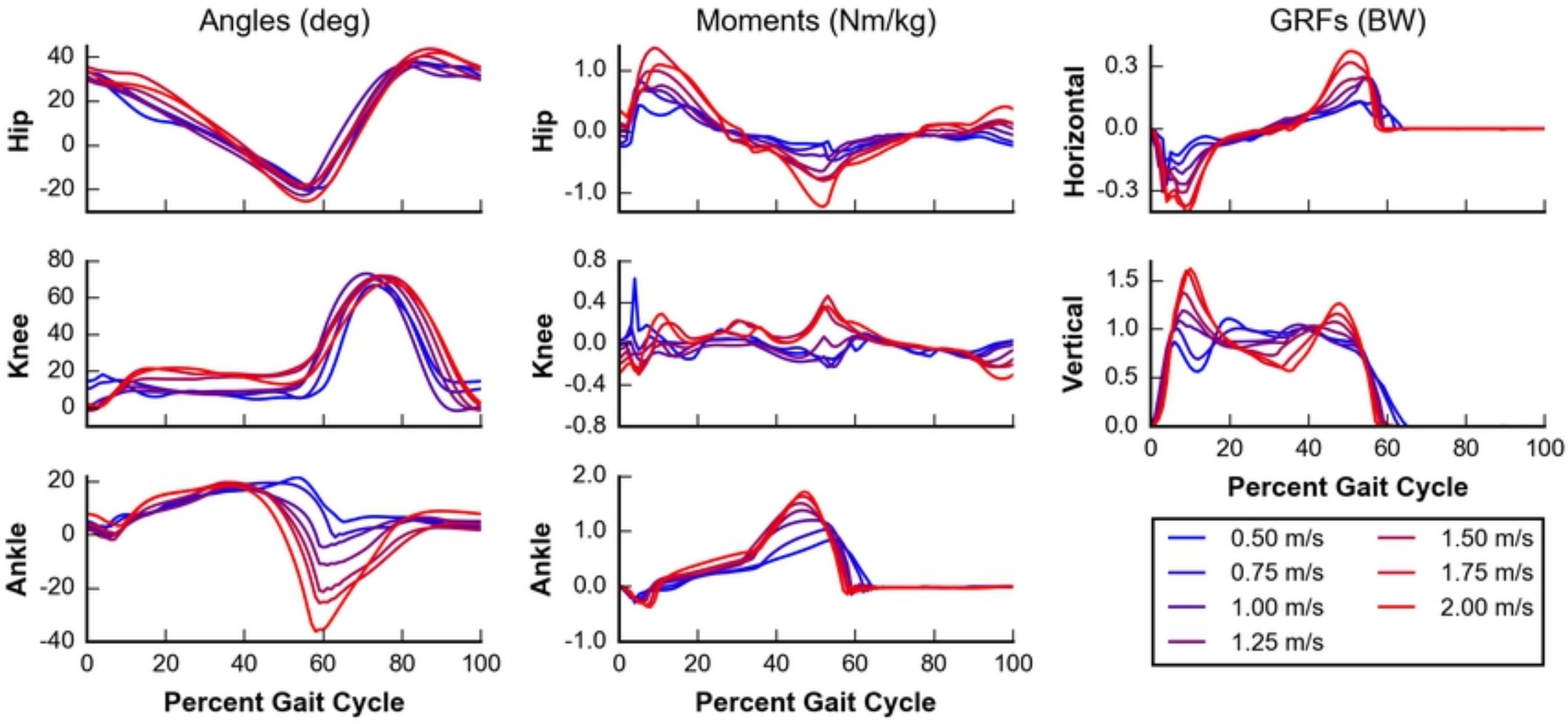
Angles (deg)
Moments (Nm/kg)
GRFs (BW)
Hip
Knee
Ankle
Horizontal
Vertical
Percent Gait Cycle
0.50 m/s
0.75 m/s
1.00 m/s
1.25 m/s
1.50 m/s
1.75 m/s
2.00 m/s

Figure 2

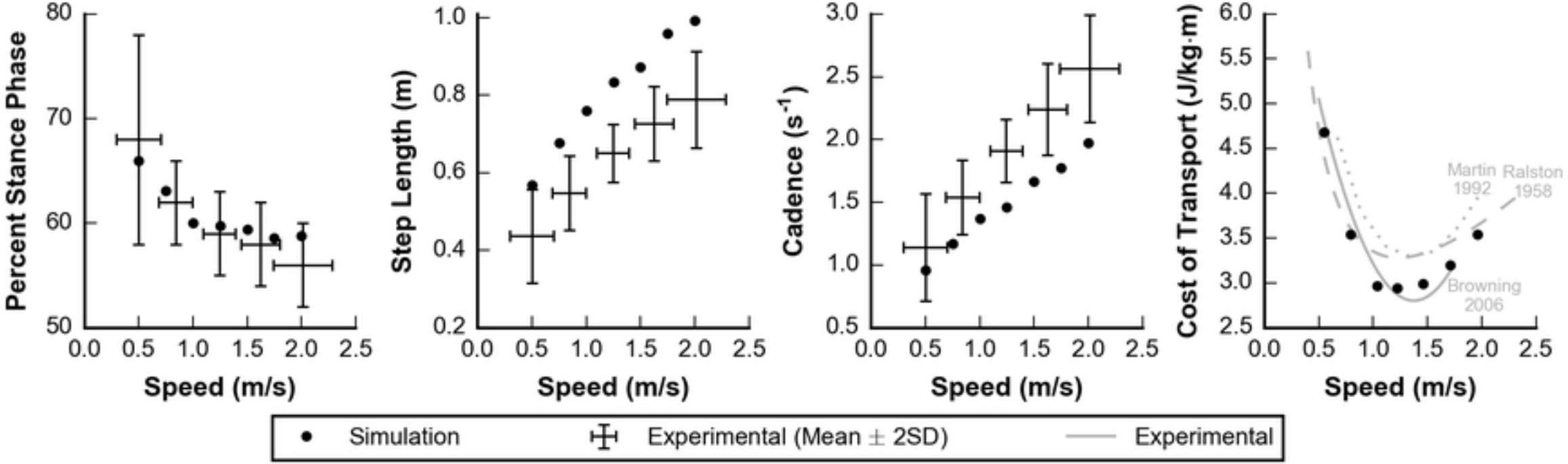
Percent Stance Phase
Speed (m/s)
Step Length (m)
Speed (m/s)
Cadence (s-1)
Speed (m/s)
Cost of Transport (J/kg·m)
Speed (m/s)
Martin 1992
Ralston 1958
Browning 2006
Simulation
Experimental (Mean ± 2SD)
Experimental

Figure 3

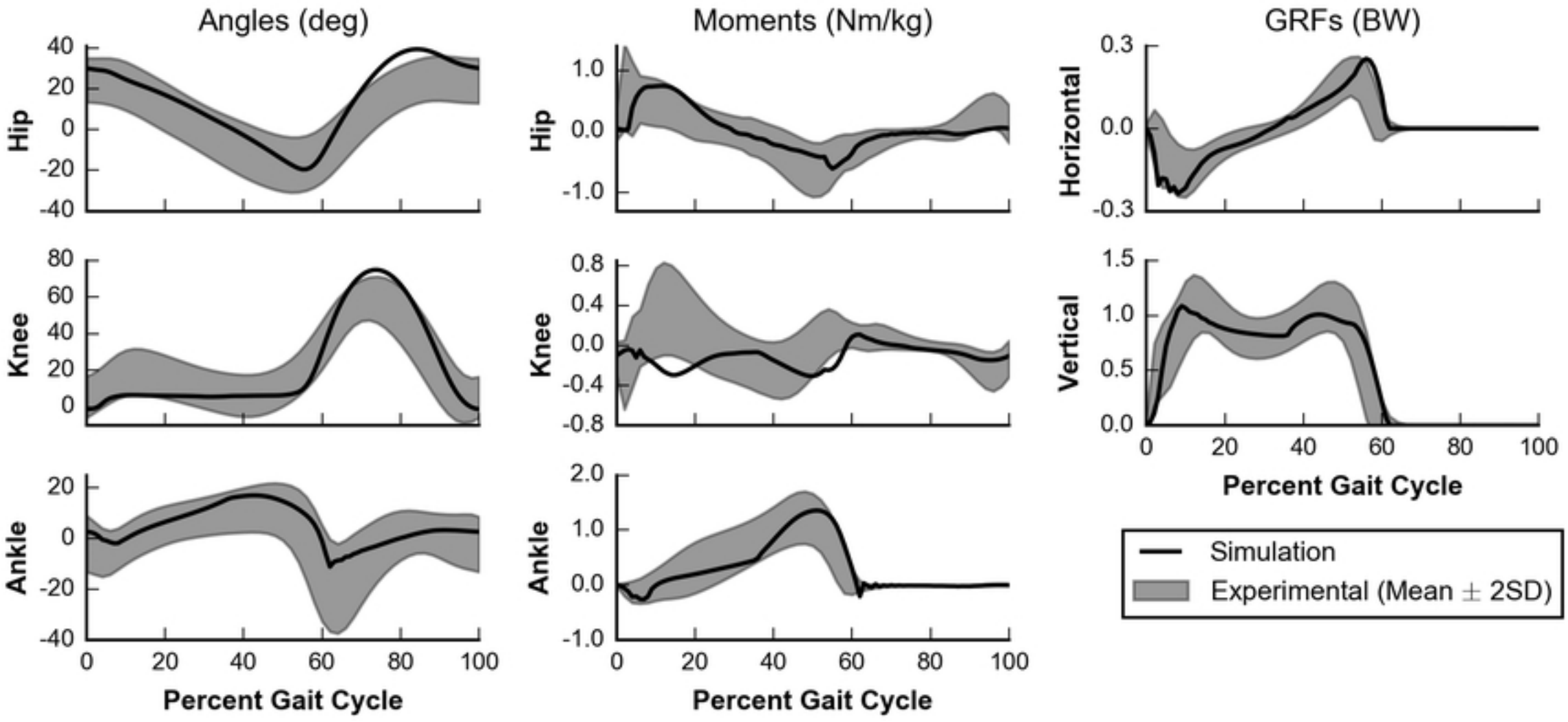
Angles (deg)
Moments (Nm/kg)
GRFs (BW)
Hip
Knee
Ankle
Horizontal
Vertical
Percent Gait Cycle
Simulation
Experimental (Mean ± 2SD)

Figure 4

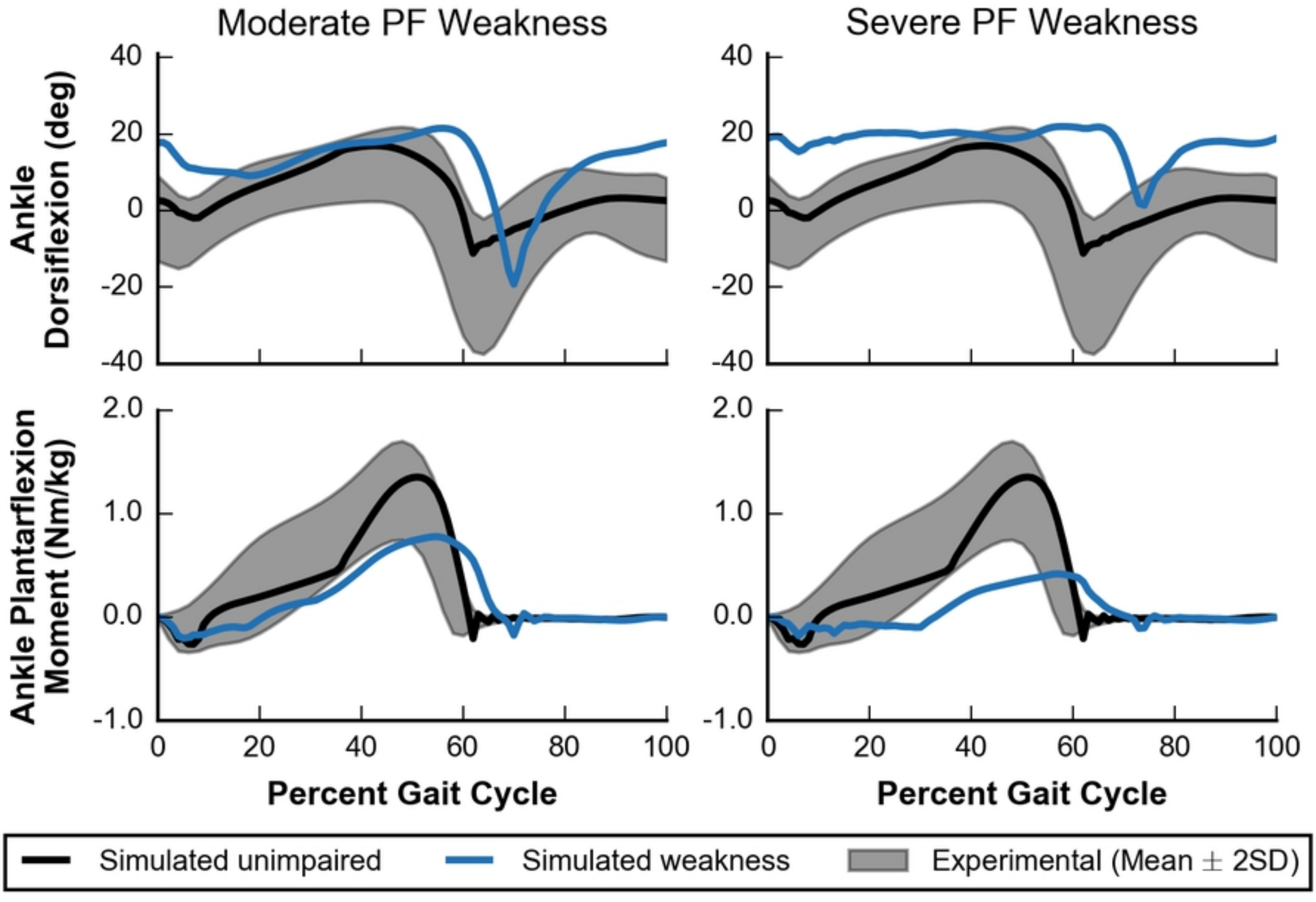
Moderate PF Weakness
Severe PF Weakness
Ankle Dorsiflexion (deg)
40
20
0
-20
-40
Ankle Plantarflexion Moment (Nm/kg)
2.0
1.0
0.0
-1.0
0
20
40
60
80
100
Percent Gait Cycle
Simulated unimpaired
Simulated weakness
Experimental (Mean ± 2SD)

Figure 6

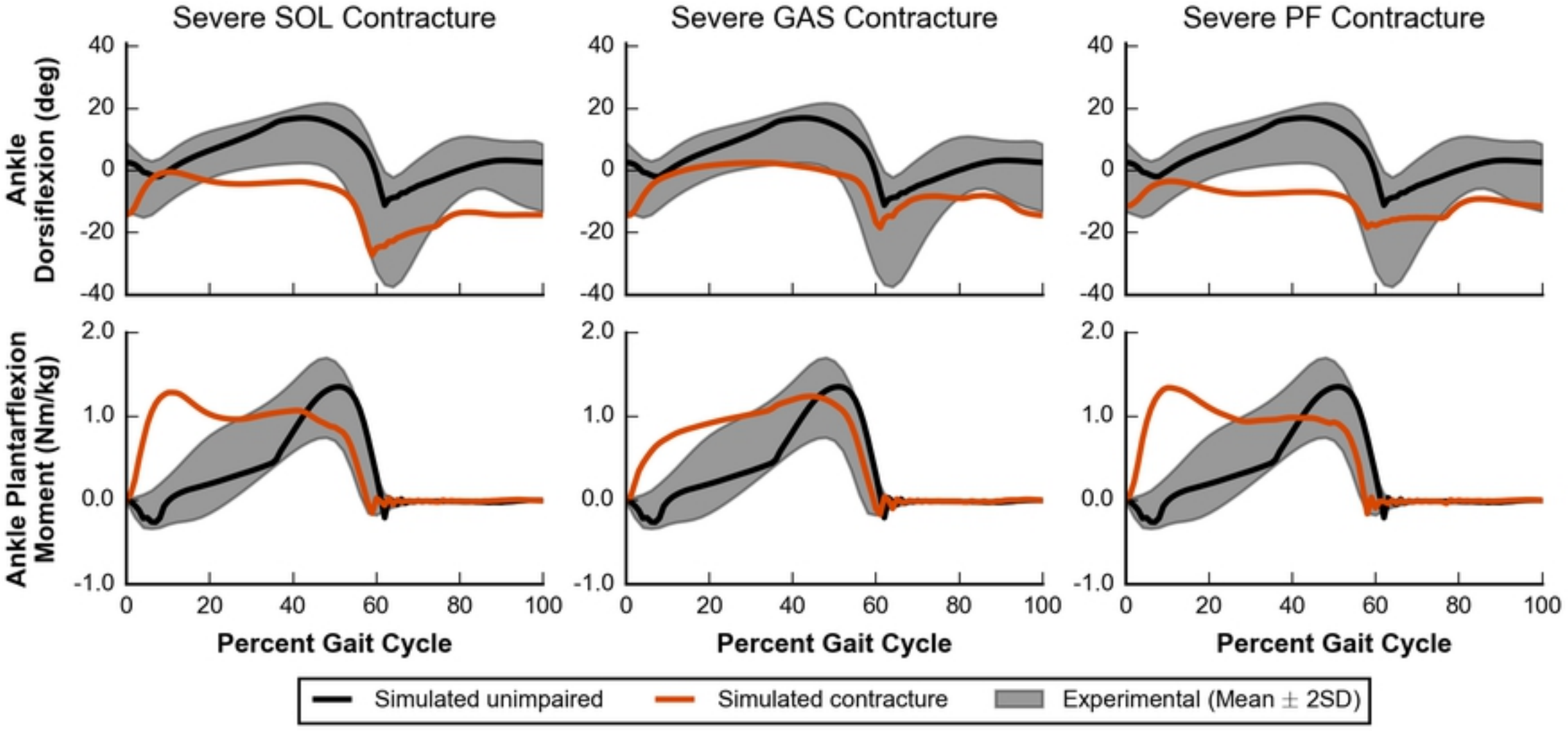
Severe SOL Contracture
Severe GAS Contracture
Severe PF Contracture
Ankle Dorsiflexion (deg)
Ankle Plantarflexion Moment (Nm/kg)
40
20
0
-20
-40
2.0
1.0
0.0
-1.0
0
20
40
60
80
100
Percent Gait Cycle
Simulated unimpaired
Simulated contracture
Experimental (Mean ± 2SD)

Figure 7

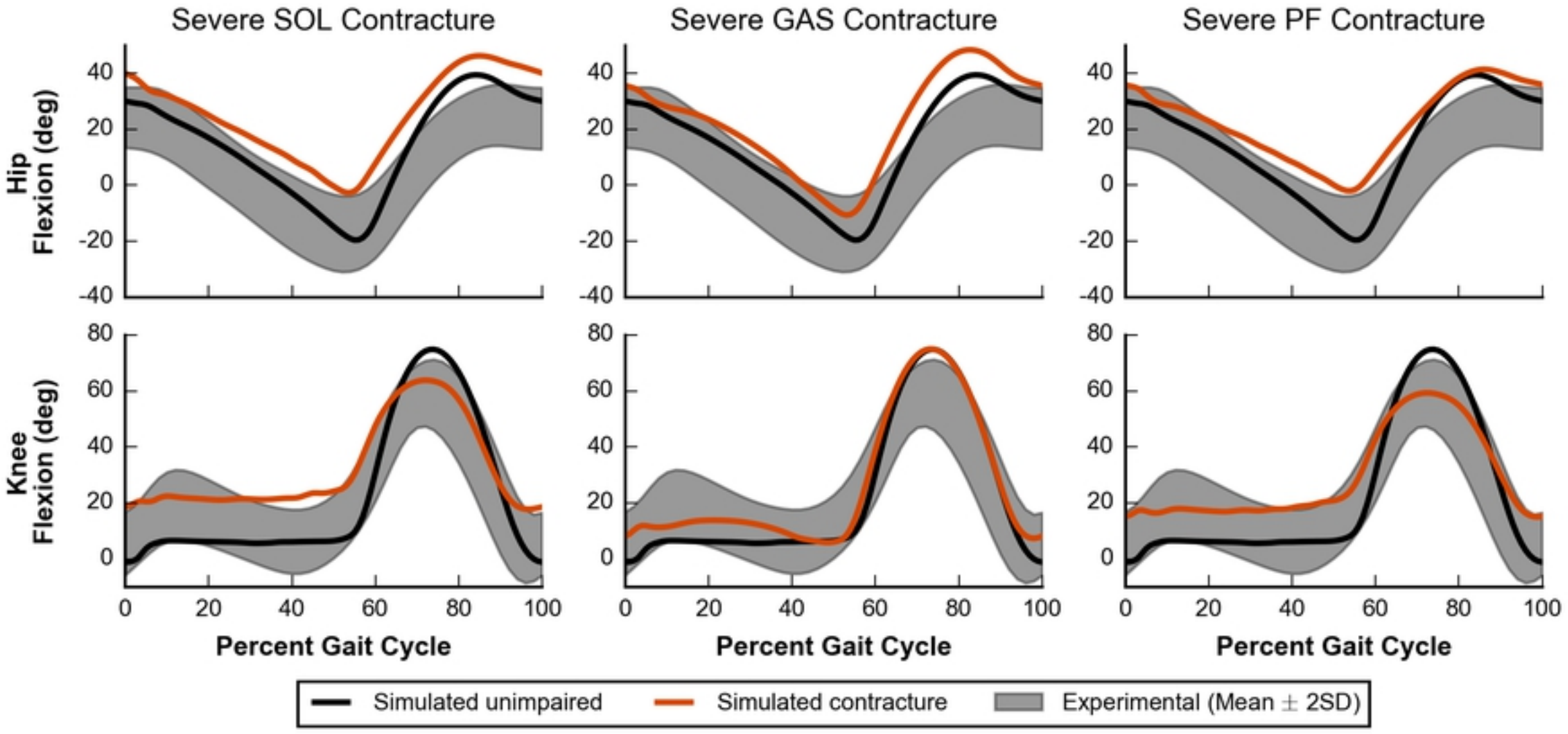
Severe SOL Contracture
Severe GAS Contracture
Severe PF Contracture
Hip Flexion (deg)
Knee Flexion (deg)
40
20
0
-20
-40
80
60
40
20
0
0
20
40
60
80
100
Percent Gait Cycle
Simulated unimpaired
Simulated contracture
Experimental (Mean ± 2SD)

Figure 8

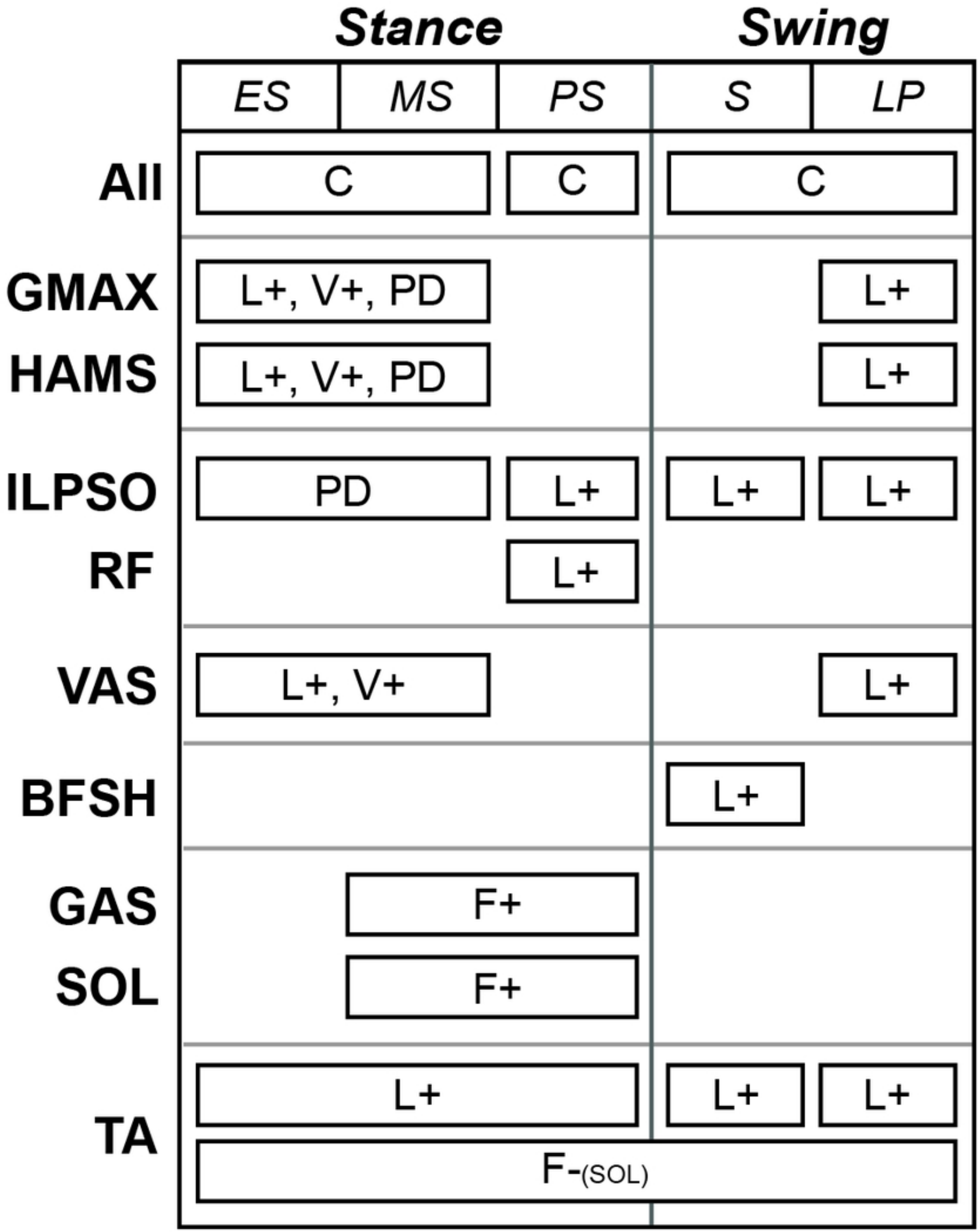
Stance
Swing
ES
MS
PS
S
LP
All
C
C
C
GMAX
L+, V+, PD
L+
HAMS
L+, V+, PD
L+
ILPSO
PD
L+
L+
L+
RF
L+
VAS
L+, V+
L+
BFSH
L+
GAS
F+
SOL
F+
TA
L+
L+
L+
F-(SOL)

Figure 10

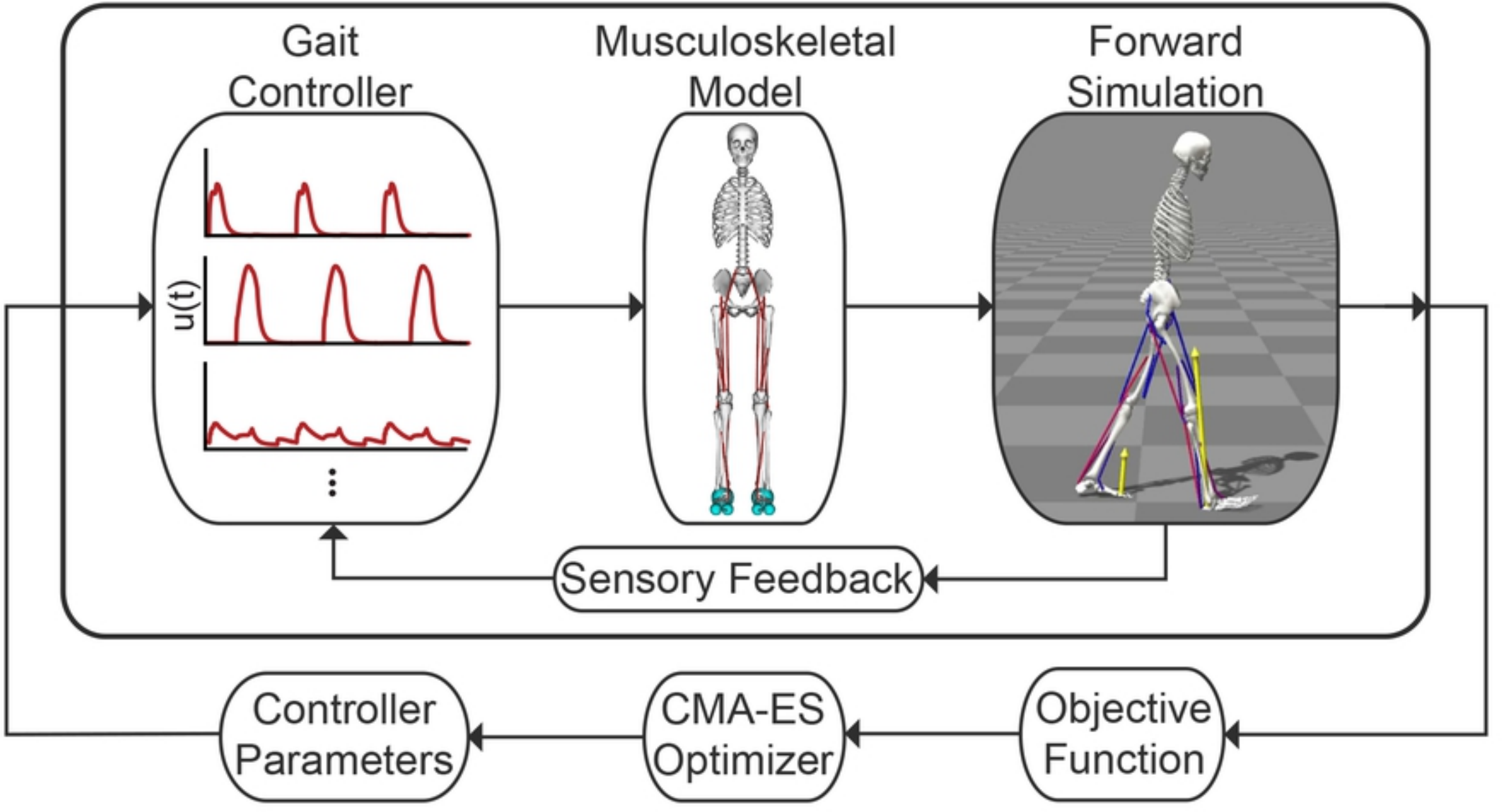
Gait
Controller
u(t)
Musculoskeletal
Model
Forward
Simulation
Sensory Feedback
Controller
Parameters
CMA-ES
Optimizer
Objective
Function

Figure 1

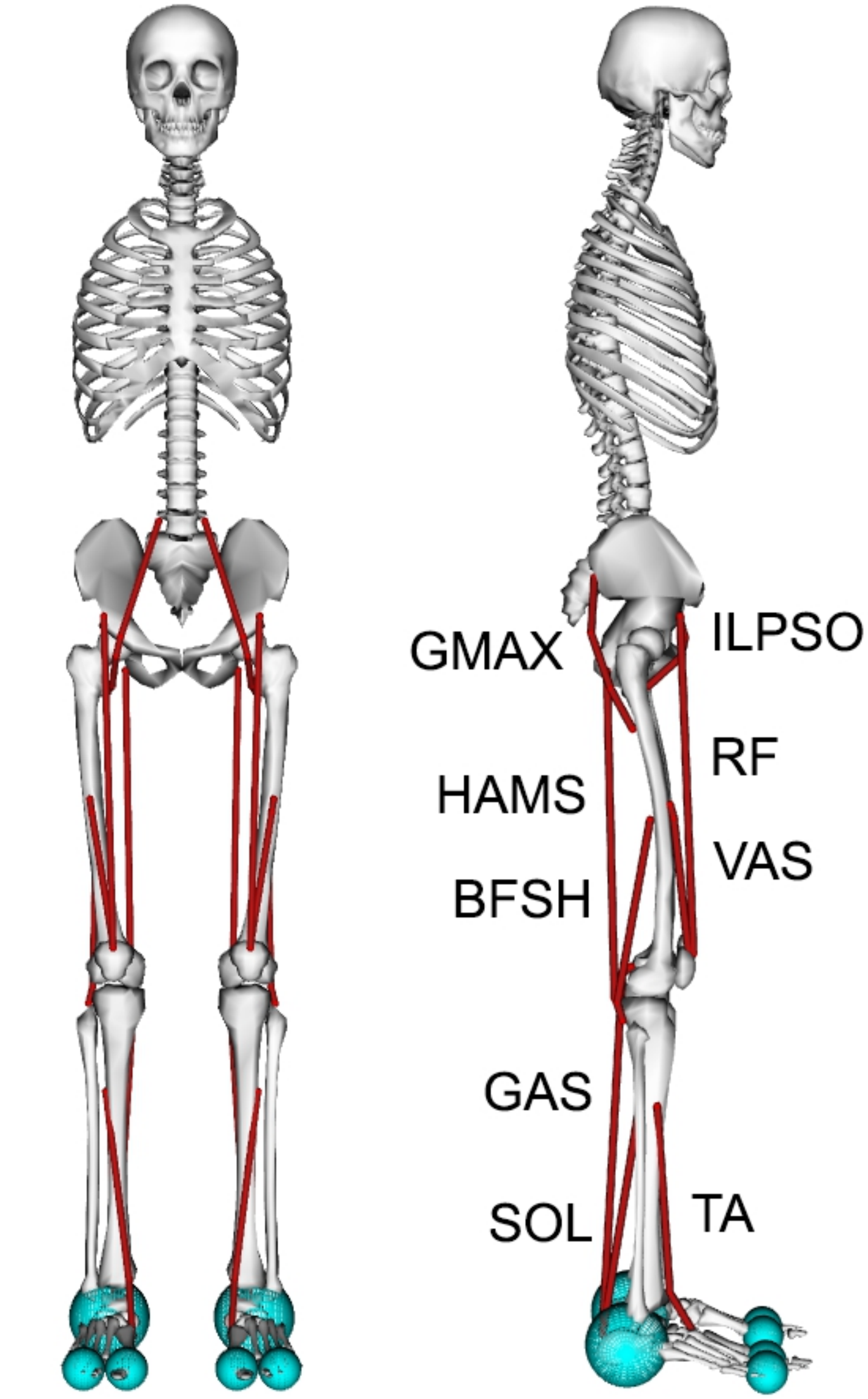

Figure 9

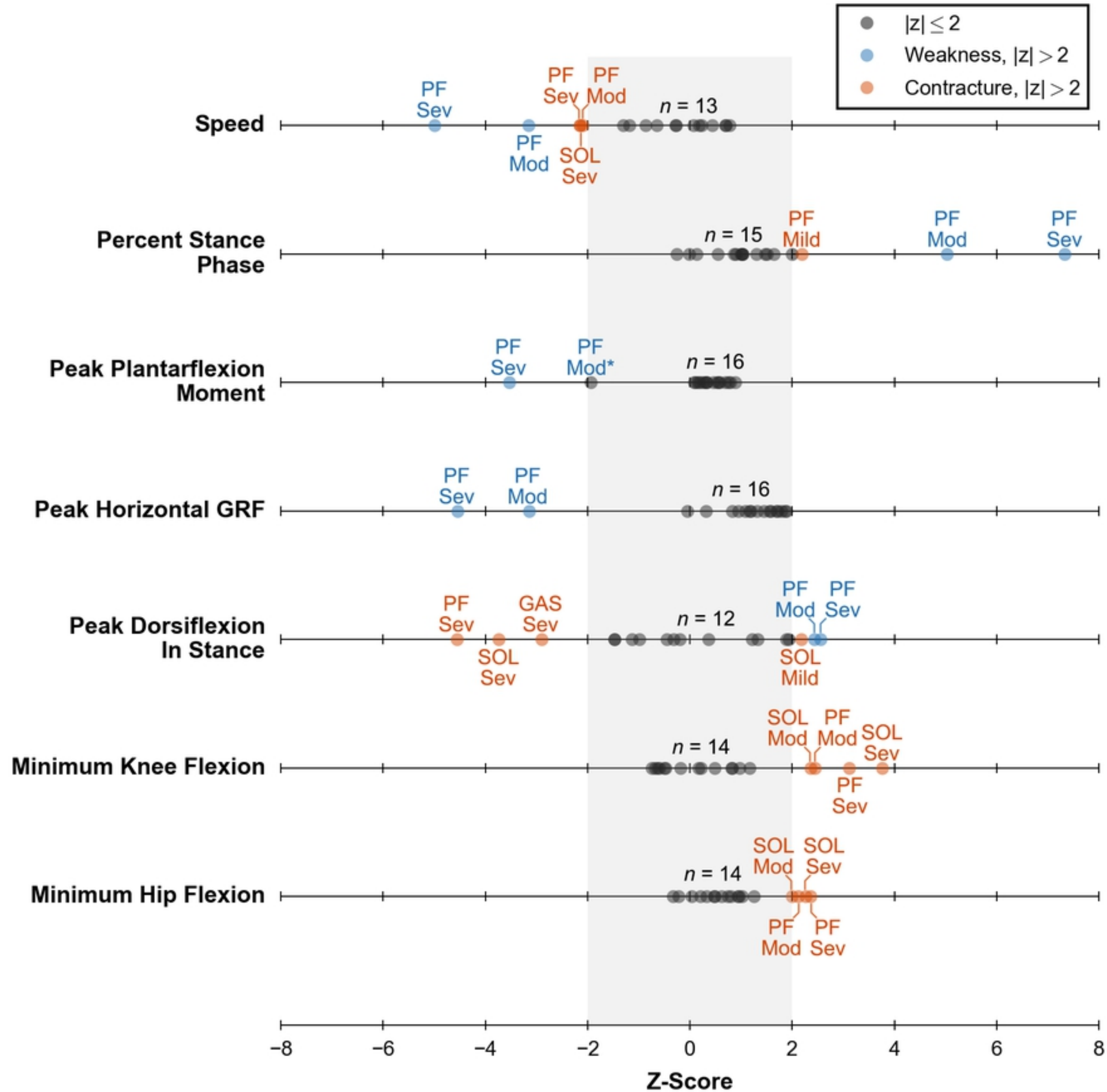
|z| ≤ 2
Weakness, |z| > 2
Contracture, |z| > 2
Speed
PF Sev
PF Mod
PF Sev
PF Mod
SOL Sev
n = 13
Percent Stance Phase
n = 15
PF Mild
PF Mod
PF Sev
Peak Plantarflexion Moment
PF Sev
PF Mod*
n = 16
Peak Horizontal GRF
PF Sev
PF Mod
n = 16
Peak Dorsiflexion In Stance
PF Sev
SOL Sev
GAS Sev
n = 12
PF Mod
PF Sev
SOL Mild
Minimum Knee Flexion
n = 14
SOL Mod
PF Mod
SOL Sev
PF Sev
Minimum Hip Flexion
n = 14
SOL Mod
SOL Sev
PF Mod
PF Sev
−8
−6
−4
−2
0
2
4
6
8
Z-Score

Figure 5